This is an *Accepted Manuscript*, which has been through the Royal Society of Chemistry peer review process and has been accepted for publication.

Accepted Manuscripts are published online shortly after acceptance, before technical editing, formatting and proof reading. Using this free service, authors can make their results available to the community, in citable form, before we publish the edited article. We will replace this *Accepted Manuscript* with the edited and formatted *Advance Article* as soon as it is available.

You can find more information about *Accepted Manuscripts* in the **Information for Authors**.

Please note that technical editing may introduce minor changes to the text and/or graphics, which may alter content. The journal's standard **Terms & Conditions** and the **Ethical guidelines** still apply. In no event shall the Royal Society of Chemistry be held responsible for any errors or omissions in this *Accepted Manuscript* or any consequences arising from the use of any information it contains.

ARTICLE TYPE

Facile morphological control of fluorescent nano/microstructures via self-assembly and phase separation of trigonal azobenzenes showing aggregation-induced emission enhancement in polymer matrices

Mina Han,[*a,b] **Yukikazu Takeoka**[a] **and Takahiro Seki**[a]

We report a facile and mild strategy for constructing diverse fluorescent nano/microstructures via self-assembly and phase separation of trigonal azobenzene chromophores (3N1s) showing aggregation-induced emission enhancement (AIEE) in polymer matrices [poly(methyl methacrylate) (PMMA) and/or
10 poly(4-chlorostyrene) (PSCl)]. Thermal treatment above the glass transition temperature enhances the large-scale molecular motions of the polymer chains, which causes AIEE-active 3N1 molecules to assemble into fluorescent nanorods and long nanosticks in the confined homopolymer (PMMA and PSCl, respectively) matrices. Strikingly, as-prepared 3N1/PMMA/PSCl ternary mixtures exhibit a splendid raspberry-like morphology. In other words, the uneven island-like surfaces with micrometer-scale round
15 protuberances are decorated with red fluorescent nanospheres. This result can be interpreted as surface-directed phase separation of immiscible PMMA and PSCl during quick solvent evaporation, which would help the 3N1 components instantaneously assemble into nanospheres on uneven surfaces. By annealing above the glass transition temperature, a distinct morphological transformation from a raspberry-like to a bead-like structure could readily be visualized via (i) the inherent assembly of 3N1 molecules into red
20 fluorescent spherical or 1D aggregates and (ii) the selective fluorescence marking due to the difference in compatibility between 3N1 and PMMA or PSCl.

Introduction

Fluorescent organic spherical or one-dimensional (1D) nano/microstructures have received increasing attention over the
25 past decade because of their applications in both biomedical materials and optoelectronic devices for organic transistors, light emitting diodes, 1D lasing, optical waveguides, solar cells, etc.[1,2] Common methods for preparing organic 1D nano/microstructures include vapor-deposition,[3] template-assisted synthesis,[4] and self-
30 assembly.[5] In particular, the molecular self-assembly of small functional components into supramolecular architectures requires neither templates nor auxiliaries, but rather is driven via weak noncovalent interactions, including π–π stacking, van der Waals and hydrogen bonding interactions.[6] Thus, the morphologies of
35 self-assembled nanostructures are significantly influenced by not only the molecular structure (including electronic and steric factors) but also weak intermolecular interactions.

Polymer blends have a number of practical applications due to their potential to improve individual homopolymer attributes and
40 develop functional composite materials.[7-9] The surface chemical composition of polymer blends differs from the bulk composition due to the active thermal molecular motions of polymer chains in the asymmetrical environment at the air-polymer interface. Their morphologies can be determined via the selective migration of
45 minor functional components[8f] or a polymer with the lowest

surface free energy to the surface. Recently, Moffitt *et al.*[8c-8e] developed a strategy for the fast and efficient patterning of photoluminescent quantum dots in polymer films via spinodal decomposition and selective wetting of polymer mixture
50 components. Ihara *et al.*[2j,2k] reported an energy-transfer spectral conversion process in a phase-separated nanodomain (induced via self-assembly of fluorescent organic gelators) in a polymer matrix. Their approach for using phase-separated nanodomains has an advantage of modulating emission wavelength and efficient
55 fluorescence resonance energy transfer.

We have recently synthesized a distorted trigonal azobenzene chromophore (3N1, Scheme 1) that exhibits aggregation-induced emission enhancement (AIEE).[10] In a previous report, we described that 3N1 has a strong tendency to assemble into
60 fluorescent crystalline nanofibers in aqueous solution.[10a] Our detailed investigations revealed that partially increased planarization and inclined arrangements of the chromophores are responsible for the increase in fluorescence efficiency in the crystalline state. The shape and size control of 1D nanostructures,
65 such as rods, sticks, wires, and belts, is of great interest because they can serve as building blocks and offer better stability, conductivity, charge transport, and optoelectronic performance.[1,2] Nevertheless, tailoring their size and shape is difficult because the nanofibers are prone to form entangled agglomerates and
70 consequently separate from the solvent during storage.

An understanding of how the desired size, shape and spatial distribution of the nanostructures assembled from such functional organic components are controlled in polymer matrices would help us to develop new functional
5 nanomaterials. In this context, here we describe a facile approach for constructing diverse self-assembled architectures with a specific size and morphology. Thermal treatment accelerates large-scale molecular motions of polymer chains and self-assembly of AIEE-active 3N1 molecules into fluorescent
10 rods and sticks in the confined homopolymer [poly(methyl methacrylate) (PMMA) and poly(4-chlorostyrene) (PSCl)] matrices, respectively. Especially, 3N1/PMMA/PSCl ternary mixture films display a marked change from a raspberry-like to a bead-like structure upon annealing above the glass transition
15 temperatures.
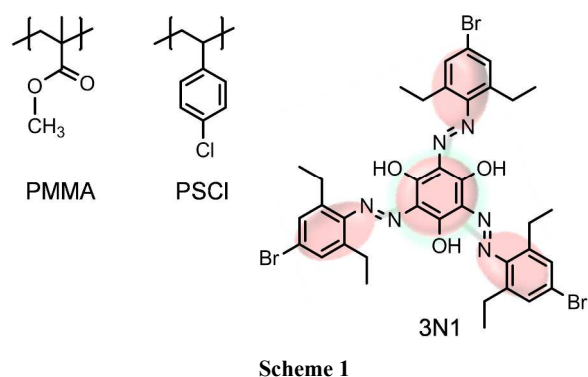
Results and Discussion

We have employed AIEE-active 3N1 (containing Br and N), PMMA, and PSCl (containing Cl) instead of polystyrene (PS containing only C and H) in this investigation. These specific
20 elements (Br, N and Cl) were chosen with the intention of efficiently identifying and analyzing phase-separated domains by energy dispersive X-ray spectroscopy (EDS). The two polymers have similar glass transition temperatures (T_g of 105 °C and 110 °C, respectively). We dissolved 3N1 and PMMA (or PSCl) in
25 chloroform (3N1: polymer = 1:10, w/w) and cast the transparent solution onto clean quartz and glass substrates. The film thicknesses were determined to be approximately 0.5–5 μm based on cross-sectional scanning electron microscopy (SEM) experiments.
30 Unlike homogeneous optical microscopy (OM) and corresponding fluorescence optical microscopy (FOM) images for the as-prepared 3N1/PMMA mixed films (Fig. 1a and 1b), annealing at 180 °C for 30 min led to the formation of a large number of red fluorescent rod-like aggregates (Fig. 1c and 1d).
35 The surface and cross-sectional SEM observations (Fig. 1e and 1f) provide convincing evidence that cylindrical rods 100–500 nm wide and less than 5 μm long are dispersed throughout the PMMA matrix. Their size and shape scarcely depended on the annealing temperatures ranging from 120 °C to 198 °C (above the
40 glass transition temperature). Evidently, the nanorods protrude from loose PMMA holes (Fig. 1f), which presumably arise from the poor compatibility between 3N1 and PMMA in the solid state.

For comparison, 3N1 and PSCl, which seems to be more
45 compatible with 3N1 than PMMA, were dissolved in chloroform, and the mixed solution was cast onto glass and quartz substrates. The surface and cross-sectional SEM images show that the annealed 3N1/PSCl film contains even longer sticks with lengths ranging from several to tens of micrometers (inset of Fig. 2a),
50 which is in good agreement with the FOM image in Fig. 2b. In contrast to the short nanorods within loose PMMA holes, these longer sticks (Fig. 2a and 3a) as well as distinguishable nanoaggregates less than 50 nm in size stick tightly to the PSCl matrix, which is most likely attributable to the good compatibility
55 between 3N1 and PSCl.

Scheme 1
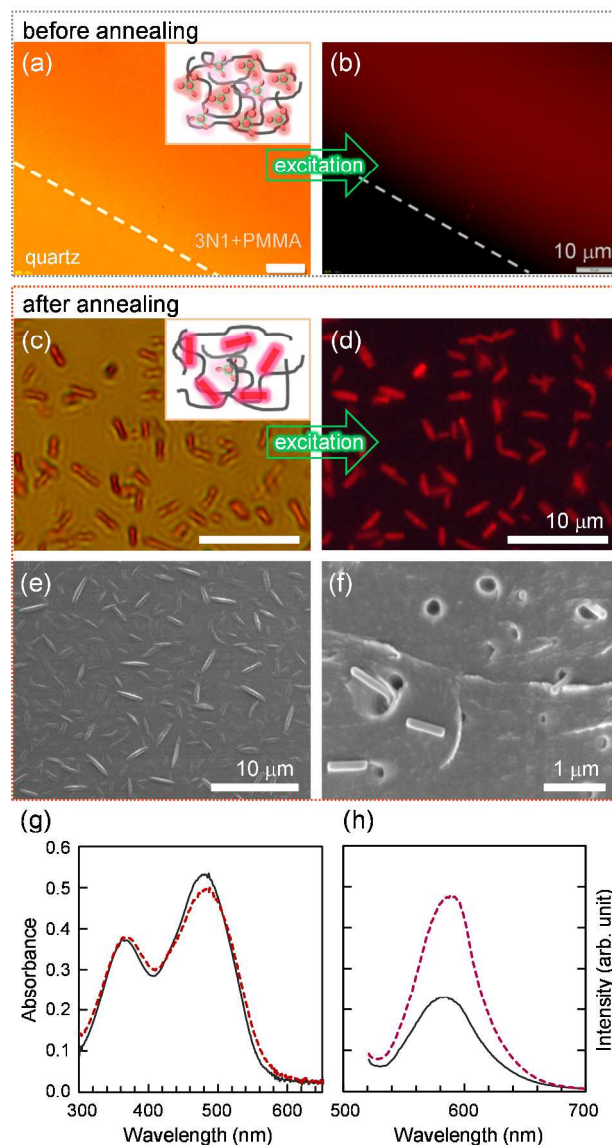
Fig. 1 Characterization of a 3N1/PMMA film (a, b) before and (c-f) after annealing at 180 °C for 30 min. The images were obtained via (a, c) OM, (b, d) FOM (λ_{ex} = 520–550 nm), and both (e) surface and (f) cross-sectional SEM. Loose and empty voids are clearly visible in the cross-sectional SEM image shown in Fig. 2f. (g) UV-vis absorption and (h) uncorrected fluorescence spectra. The black and red lines correspond to before and after thermal treatment,
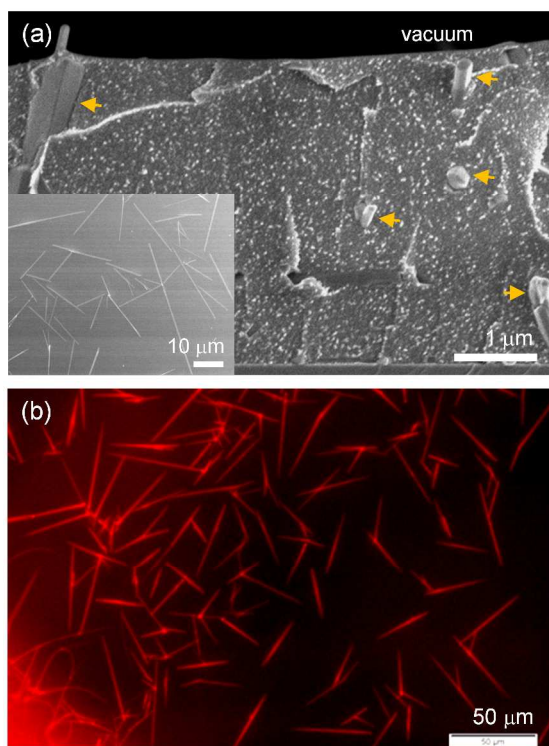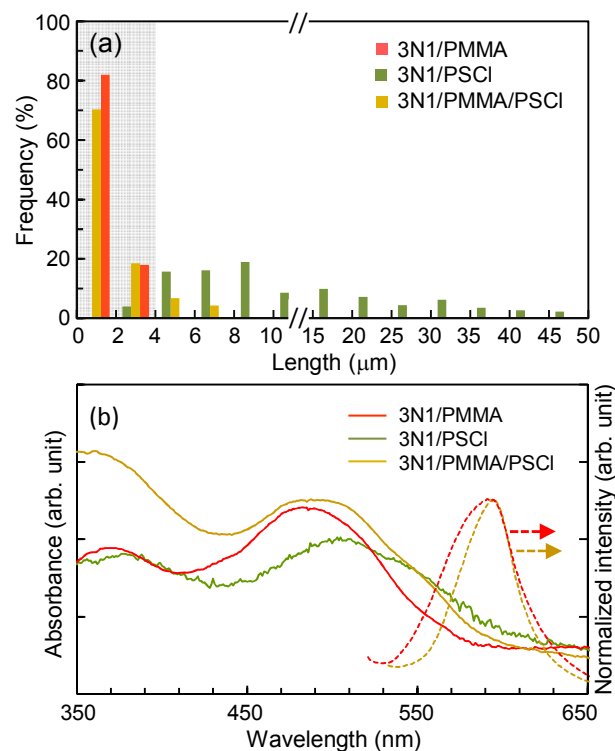
Fig. 2 (a) Cross-sectional and surface (inset) SEM and (b) FOM images of a 3N1/PSCl mixture film annealed at 198 °C for 30 min.

Fig. 3 (a) Length distributions for the 1D structures observed from the SEM and OM images of the annealed films. (b) UV-vis absorption and fluorescence spectra of annealed mixture films. The red and yellow dashed lines correspond to fluorescence from the annealed 3N1/PMMA and 3N1/PMMA/PSCl films, respectively.

Fig. 1g shows the changes in the absorption spectra before and after annealing the 3N1/PMMA film. The as-prepared 3N1/PMMA film exhibits two intense absorption bands with maxima at 363 and 477 nm, which can be assigned to the $\pi-\pi^*$
5 transition of the azobenzene unit and the energetically similar (π,π^*) and (n,π^*) states, respectively.[10a] These positions are quite comparable to those (362 and 476 nm) of a dilute 3N1 solution. This experimental observation can be explained as follows: Upon casting the 3N1/homopolymer mixed solution, quick evaporation
10 of the volatile chloroform rapidly freezes the sample and prevents any appreciable 1D growth of the 3N1 molecules. That is, the 3N1s are quite homogeneously dispersed over a microscopic range throughout the frozen polymer matrix, as evidenced by Fig. 1a and 1b.
15 Upon annealing the 3N1/PMMA film, the emission wavelength was red-shifted from 585 nm to 590 nm when excited at 500 nm (Fig. 1h). The fluorescence quantum yield of 3N1 $(\Phi_f \sim 0.002)$[10a] increased by 2-3 times. When compared with a slight red-shift in the absorption bands to 369 and 483 nm for the
20 annealed 3N1/PMMA film, much larger red-shifts were observed to 377 and 503 nm for the annealed 3N1/PSCl mixed film (Fig. 3b). These spectral changes are probably due to the formation of short nanorods and longer sticks via inclined arrangements (i.e., J-aggregation) of the trigonal azobenzene chromophores in the
25 polymer matrices.[11]

Thermal treatment gives rise to the large-scale molecular motions of the polymer chains, which allows neighboring 3N1 molecules to interact with one another via $\pi-\pi$ stacking. Consequently, the 3N1 molecules stack into relatively short

30 cylindrical rods and sticks in the confined homopolymer (PMMA and PSCl) matrices, respectively, instead of elongated fibers.

We next prepared 3N1/PMMA/PSCl (1:2:8) ternary mixture films from the corresponding chloroform solution to examine how the 3N1 assembly is affected by phase separation in an
35 immiscible PMMA/PSCl mixture system. Unexpectedly, for the as-prepared sample, a raspberry-like morphology was observed in the FOM image (Fig. 4a). The laser confocal microscopy (LCM) image shown in Fig. 4b offers direct evidence that uneven island-like surfaces with micrometer-scale round protuberances are
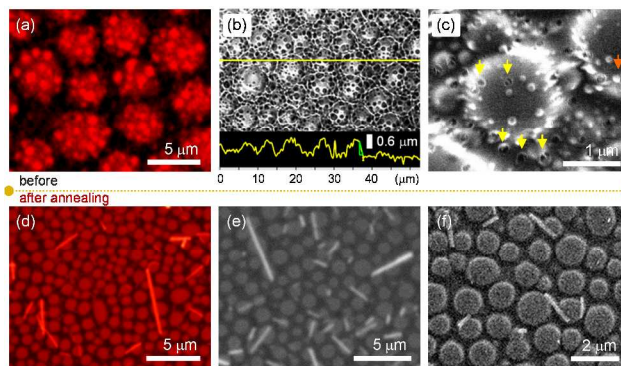
Fig. 4 Characterization (a-c) before and (d-f) after annealing 3N1/PMMA/PSCl (1:2:8) ternary mixtures at 198 °C for 30 min. The images were obtained via (a, d) FOM ($\lambda_{ex} = 520$–550 nm), (b, e) LCM, and (c, f) SEM.
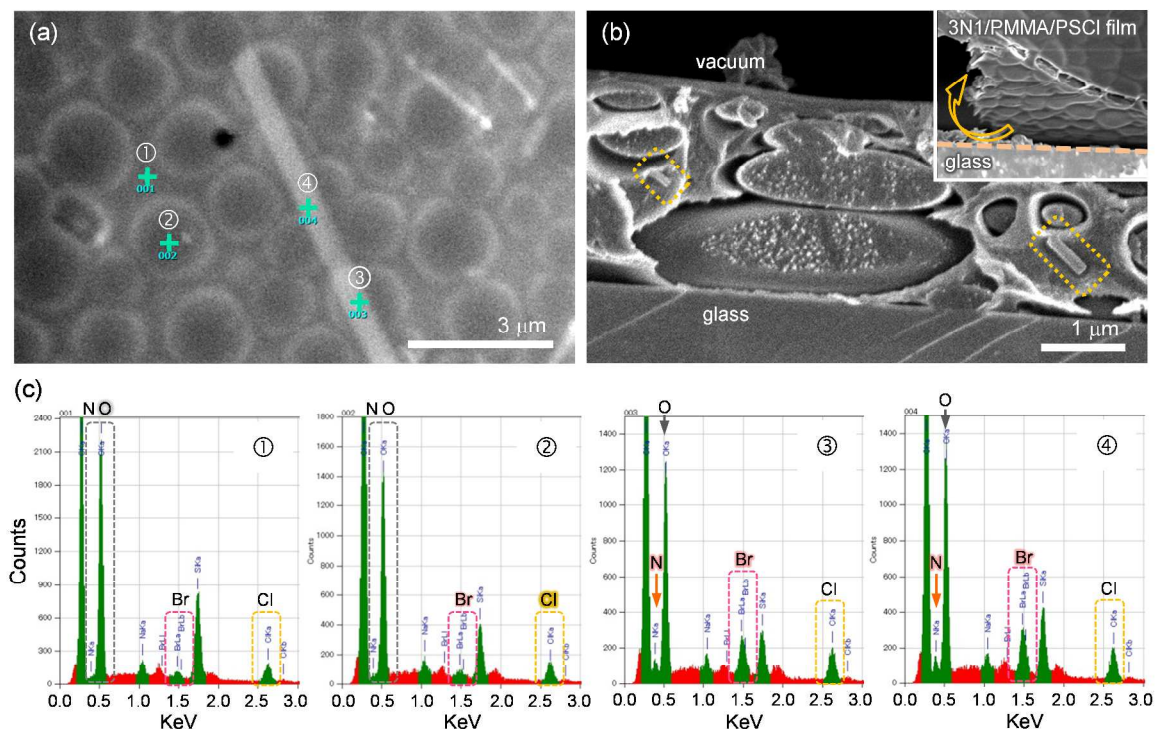
Fig. 5 (a) Surface and (b) cross-sectional SEM images of annealed 3N1/PMMA/PSCl films. (c) EDS spectra corresponding to four points (1-4) on the surface SEM image (Fig. 5a).

decorated with red fluorescent nanospheres 50–200 nm in diameter. Clearly, the magnified SEM image (Fig. 4c) confirms the existence of not only nanospheres detached from round holes (orange arrows) but also empty holes (yellow arrows), which are most likely due to the high vacuum required for the SEM sample preparation.

This splendid morphology seems to result from both the rapid surface-directed phase separation of the PMMA and PSCl and the resultant instantaneous assembly of 3N1 molecules into nanospheres on the surface.[8f] That is, the considerably restricted molecular motion for the polymer segments due to the quick solvent evaporation prevents the 3N1 molecules from further growing into long 1D structures. Eventually, the growth stops at the nanosphere level.

Notably, thermal treatment led to a drastic change in the blend morphology. The raspberry-like structure disappears completely, and the surface becomes smooth with no defined structures (Fig. 4d-4f and 5). The FOM, LCM, and SEM images show that the annealed 3N1/PMMA/PSCl film contains three different phases: (i) red fluorescent cylindrical rods, (ii) fluorescent micrometer-scale bead-like structures, and (iii) dark surrounding matrices.

We performed surface SEM and EDS measurements to analyze the elemental composition of the respective phases. The penetration depth for a 10–15 kV electron beam is expected to be approximately 2 μm.[12] Therefore, the EDS method collects both surface and depth information. Fig. 5c shows the respective EDS data corresponding to four points (1–4) in the SEM surface image (Fig. 5a). While the atomic [Br]/[Cl] ratio (percentage number of atoms) was found to be 8.9 and 8.3 for 1 and 2, respectively, points 3 and 4 in the 1D structure contained significantly more Br and N (only from 3N1) than Cl (only from PSCl). The [Br]/[Cl]
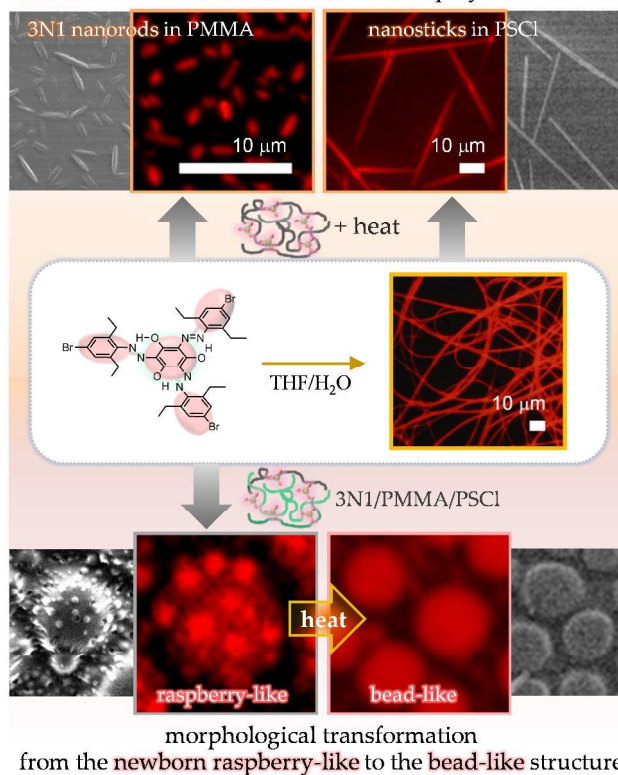
Fig. 6 Formation and visualization of self-assembled morphologies via self-assembly and phase separation of AIEE-active 3N1 molecules in polymer matrices.

ratio (percentage number of atoms) was estimated to be 36.8 and 45.6 for 3 and 4, respectively. Accordingly, we conclude that the red fluorescent rods (3 and 4) are primarily produced via the assembly of 3N1 molecules. Nevertheless, it is still difficult to confirm that points 1 and 2 correspond to PMMA and PSCl, respectively, because of the electron beam penetration depth and phase-separated domains in the bulk regions.

Alternatively, the cross-sectional SEM images in Fig. 5b indicates that the matrix surrounding the bead-like domains and thin bottom layer is mainly composed of PMMA.[13,14] That is, as the sample evolves towards thermodynamic equilibrium during the thermal treatment, the PSCl forms bead-like structures on top of a PMMA bottom layer that wets the hydrophilic SiOx substrate, as expected from the previous report by Harris *et al.*[7d] Noticeably, Fig. 5b displays that a large number of nanoaggregates comparable to those observed in the 3N1/PSCl mixture (Fig. 2a) stick to the bead-like PSCl domains. Considering the compatibility difference of 3N1 with PMMA and PSCl, it is reasonable that 3N1 is favorably delivered to the more congenial PSCl phase. As a consequence, the bead-like PSCl domains are distinguished from the PMMA domain by the selective fluorescence marking.

Conclusions

While the AIEE-active 3N1 molecules are quite homogenously dispersed in the as-prepared 3N1/homopolymer (PMMA or PSCl) mixed films, thermal treatment causes the 3N1 molecules to assemble into relatively short rods and even longer sticks in the confined PMMA and PSCl matrices, respectively (Fig. 6). In stark contrast, for the 3N1/PMMA/PSCl ternary blend, the restricted molecular motion and surface-directed phase separation of mixed PMMA and PSCl significantly affect the 3N1 assembly and spatial variation, which results in the formation of a unique raspberry-like surface morphology decorated with fluorescent nanospheres. Thermal treatment above the glass transition temperatures leads to large-scale phase separation and the selective migration of 3N1 molecules toward congenial PSCl domains with a resultant fluorescence marking, eventually producing the morphological transformation from the raspberry-like structure to the bead-like structure. This facile construction strategy for developing fluorescent nano/microstructures has important implications for guiding new luminescent polymer composite materials capable of operating as polymer-based light-emitting devices, antireflection coatings, and biocompatible membranes.

Experimental Section

Materials

A detailed synthetic procedure for 3N1 is described in a previous work.[10a] Poly(methyl methacrylate) (PMMA, M_w = 996,000, T_g = 105 °C) and poly(4-chlorostyrene) (PSCl, M_w = 250,000, T_g = 110 °C) homopolymers were purchased from Aldrich. PMMA, PSCl and 3N1 mixtures were prepared by dissolving each component in spectroscopic grade chloroform to polymer concentrations of 5 and 10 wt%. The mixtures were stirred for 30 min to obtain transparent solutions.

Instrumentation

Optical microscopy (OM), fluorescence optical microscopy (FOM, λ_{ex} = 520–550 nm), and laser confocal microscopy (LCM) images were obtained using an Olympus BX51 microscope and LEXT OLS4000 3D laser microscope (λ_{ex} = 405 nm) after placing a few drops of the 3N1 suspension on a quartz substrate cleaned with KOH/ethanol. Absorption and fluorescence spectra were obtained using an Agilent 8453 diode array spectrometer and JASCO FP-8500 spectrofluorometer, respectively. A JEOL JSM-7500FA field-emission scanning electron microscope (FE-SEM) operating at 2 kV was used to investigate the morphologies of the films after coating with approximately 10 nm of osmium using a Filgen osmium plasma coater (OPC60A). Energy dispersive X-ray spectroscopy (EDS) operating from 10–15 kV was used to determine the elemental compositions of the films.

Notes and references

[a] Department of Molecular Design & Engineering, Nagoya University, Furo-cho, Chikusa-ku, Nagoya 464-8603, Japan.
[b] Present Address: Department of Chemistry and Biotechnology, Tottori University, 4-101 Koyama Minami, Tottori 680-8552, Japan. Tel: 81 857 31 5331; E-mail: hanmin@chem.tottori-u.ac.jp

1   (a) L. Palmer and S. Stupp, *Acc. Chem. Res.*, 2008, **41**, 1674; (b) Y. Zhao, H. Fu, A. Peng, Y. Ma, Q. Liao and J. Yao, *Acc. Chem. Res.*, 2010, **43**, 409; (c) J. D. Tovar, *Acc. Chem. Soc.*, 2013, **46**, 1527.

2. (a) M. Yoshio, T. Mukai, H. Ohno and T. Kato, *J. Am. Chem. Soc.*, 2004, **126**, 994; (b) D. O'Carroll, I. Lieberwirth and G. Redmond, *Nat. Nanotechnol.*, 2007, **2**, 180; (c) E. Ishow, A. Brosseau, G. Clavier, K. Nakatani, P. Tauc, C. Fiorini-Debuisschert, S. Neveu, O. Sandre and A. Léaustic, *Chem. Mater.*, 2008, **20**, 6597; (d) J. Hong, M. Um, S. Nam, J. Hong and S. Lee, *Chem. Commun.*, 2009, 310; (e) B. Yang, J. Xiao, J. Wong, J. Guo, Y. Wu, L. Ong, L. Lao, F. Boey, H. Zhang, H. Yang and Q. Zhang, *J. Phys. Chem. C*, 2011, **115**, 7924; (f) I. Martini, I. Craig, W. Molenkamp, H. Miyata, S. Tolbert and B. Schwartz, *Nat. Nanotechnol.*, 2007, **2**, 647; (g) F. Kim, G. Ren and S. Jenekhe, *Chem. Mater.*, 2011, **23**, 682; (h) S. de Rooy, S. Das, M. Li, B. El-Zahab, A. Jordan, R. Lodes, A. Weber, L. Chandler, G. Baker and I. Warner, *J. Phys. Chem. C*, 2012, **116**, 8251; (i) X. Zhang, D. Görl, V. Stepanenko and F. Würthner, *Angew. Chem. Int. Ed.*, 2014, **53**, 1270; (j) H. Jintoku, M. Yamaguchi, M. Takafuji and H. Ihara, *Adv. Funct. Mater.*, 2014, **24**, 4105; (k) H. Jintoku, M. Dateki, M. Takafuji and H. Ihara, *J. Mater. Chem. C*, 2015, DOI: 10.1039/C4TC02948H.

3. (a) Q. Tang, H. Li, Y. Liu and W. Hu, *J. Am. Chem. Soc.*, 2006, **128**, 14634; (b) R. Li, H. Li, H. Song, Q. Tang, Y. Liu, W. Xu, W. Hu and D. Zhu, *Adv. Mater.*, 2009, **21**, 1605; (c) Y. Zhao, J. Wu and J. Huang, *J. Am. Chem. Soc.*, 2009, **131**, 3158.

4. (a) C. R. Martin, L. S. Vandyke, Z. H. Cai and W. B. Liang, *J. Am. Chem. Soc.*, 1990, **112**, 8976; (b) L. Zhao, W. Yang, Y. Ma, J. Yao, Y. Li and H. Liu, *Chem. Commun.*, 2003, 2442; (c) X. Zhang, G. Yuan, Q. Li, B. Wang, X. Zhang, R. Zhang, J. Chang, C. Lee and S. Lee, *Chem. Mater.*, 2008, **20**, 6945.

5. (a) A. L. Briseno, S. C. B. Mannsfeld, C. Reese, J. M. Hancock, Y. Xiong, S. A. Jenekhe, Z. Bao and Y. Xia, *Nano Lett.*, 2007, **7**, 2847; (b) Y. K.Che, X. Yang, K. Balakrishnan, J. Zuo and L. Zang, *Chem. Mater.*, 2009, **21**, 2930; (c) D.-W. Lee, T. Kim, I.-S. Park, Z. Huang and M. Lee, *J. Am. Chem. Soc.*, 2012, **134**, 14722.

6. (a) J.-M. Lehn, *Supramolecular Chemistry*; VCH Press: New York, 1995; (b) L. F. Lindoy, I. M. Atkinson, *Self-assembly in*

Supramolecular Systems, J. F. Stoddart, Ed. Royal Society of Chemistry: Cambridge, UK, 2000.

7. (a) K. Tanaka, A. Takahara and T. Kajiyama, *Macromolecules*, 1996, **29**, 3232; (b) S. Walheim, M. Boltau, J. Mlynek, G. Krausch and U. Steiner, *Macromolecules*, 1997, **30**, 4995; (c) C. Ton-That, A. Shard, R. Daley and R. Bradley, *Macromolecules*, 2000, **33**, 8453; (d) M. Harris, G. Appel and H. Ade, *Macromolecules*, 2003, **36**, 3307.

8. (a) P. Mülleir-Buschbaum, S. A. O'Neill, S. Affrossman, M. Stamm, *Macromolecules*, 1998, **31**, 5003; (b) D. Chen, A. Nakahara, D. Wei, D. Nordlund and T. Russell, *Nano Lett.*, 2011, **11**, 561; (c) S. Harirchian-Saei, M. Wang, B. Gates and M. G. Moffitt, *Langmuir*, 2012, **28**, 10838; (d) C.-W. Wang and M. G. Moffitt, *Chem. Mater.*, 2005, **17**, 3871; (e) Y. Guo and M. G. Moffitt, *Chem. Mater.*, 2007, **19**, 6581; (f) A. Kolahchi, A. Ajji and P. Carreau, *J. Phys. Chem. B*, 2014, **118**, 6316.

9. (a) N. Gadegaard, M. J. Dalby, M. O. Riehle, A. S. G. Curtis and S. Affrossman, *Adv. Mater.*, 2004, **16**, 1857; (b) L. Li, A. Hitchcock, N. Robar, R. Cornelius, J. Brash, A. Scholl and A. Doran, *J. Phys. Chem. B*, 2006, **110**, 16763; (c) J. Zemla, M. Lekka, J. Raczkowska, A. Bernasik, J. Rysz and A. Budkowski, *Biomacromolecules*, 2009, **10**, 2101; (d) C. Sinturel, M. Vayer, M. Morris and M. A. Hillmyer, *Macromolecules*, 2013, **46**, 5399.

10. (a) M. Han, S. Cho, Y. Norikane, M. Shimizu, A. Kimura, T. Tamagawa and T. Seki, *Chem. Commun.*, 2014, **50**, 15815; (b) J. Luo, Z. Xie, J. Lam, L. Cheng, H. Chen, C. Qiu, H. Kwok, X. Zhan, Y. Liu, D. Zhu and B. Tang, *Chem. Commun.*, 2001, 1740; (c) B.-K. An, S. Kwon, S.-K. Jung and S. Y. Park, *J. Am. Chem. Soc.*, 2002, **124**, 14410; (d) M. Han and M. Hara, *J. Am. Chem. Soc.*, 2005, **127**, 10951; (e) M. Han and M. Hara, *New J. Chem.*, 2006, **30**, 223; (f) M. Han, Y. Hirayama and M. Hara, *Chem. Mater.*, 2006, **18**, 2784; (g) Y. Hong, J. W. Y. Lam and B. Z. Tang, *Chem. Soc. Rev.*, 2011, **40**, 5361; (h) B.-K. An, J. Gierschner and S. Y. Park, *Acc. Chem. Res.*, 2012, **45**, 544.

11. (a) M. Kasha, H. R. Rawls and M. Ashraf El-Bayoumi, *Pure Appl. Chem.*, 1965, **11**, 371; (b) X. Song, J. Perlstein and D. Whitten, *J. Am. Chem. Soc.*, 1997, **119**, 9144.

12. *Let's make friends with SEM!*, Hitachi High-Technologies Corporation, 2010. http://www.hitachi-hitec.com/em/

13. The polar PMMA lays on the hydrophilic SiOx substrate, which generates a continuous bottom layer.

14. (a) S. Wu, *J. Phys. Chem.*, 1970, **74**, 632; (b) A. Augsburg, K. Grundke, K. Pöschel, H. Jacobasch and A. Neumann, *Acta Polym.*, 1998, **49**, 417.

A graphical contents entry

Facile morphological control of fluorescent nano/microstructures via self-assembly and phase separation of trigonal azobenzenes showing aggregation-induced emission enhancement in polymer matrices

Mina Han, Yukikazu Takeoka and Takahiro Seki
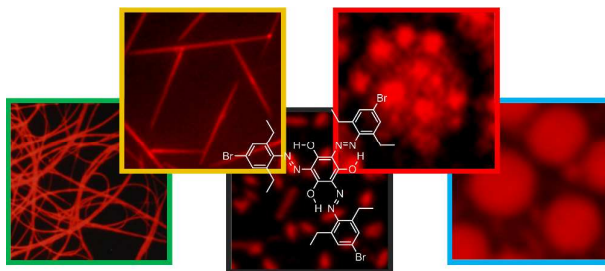
We report a facile strategy for constructing diverse nano/microstructured morphologies (nanorods, nanosticks, raspberry-like, and bead-like) via self-assembly and phase separation of trigonal azobenzene chromophores (3N1s) showing aggregation-induced emission enhancement (AIEE) in polymer matrices.